A Miniaturized Ultra-Wideband Radar for UAV Remote Sensing Applications

Feras Abushakra[1], Nathan Jeong[1], *IEEE Senior member*, Deepak N. Elluru[1], Abhishek K. Awasthi[1], *IEEE member*, Shriniwas Kolpuke[2], Tuan Luong[2], Omid Reyhanigalangashi[1], *IEEE Student member*, Drew Taylor[1], *IEEE member*, S. Prasad Gogineni[1, 2], *IEEE Life Fellow*

***Abstract*— This letter presents a novel approach to build a compact lightweight unmanned aerial vehicle (UAV) radar for remote sensing applications. The proposed radar exploits the recent advancement of an automotive radar chip for broadband chirp generation and rapid data processing. To compensate for the path losses and improve penetration at the millimeter wave (mm-wave) frequency range, an up- and down-converters are developed to generate an UWB (3.25-5.15 GHz) chirp signal. The total payload of the radar is 2.5 kg. The proposed radar is installed on a UAV and tested in the field at 100 m altitude above the ground surface. The results show that the compact low-power UWB radar can be used to map vegetation and soil moisture with fine resolution.**

***Index Terms* — FMCW Radar, linear chirp, remote sensing, Unmanned aerial vehicles (UAV).**

I. INTRODUCTION

UAV-based UWB radars exhibit great potential for remote sensing applications such as measuring snow thickness, soil moisture, and the bathymetry of rivers. They can also be used to survey agricultural fields over large areas and thereby monitor vegetation and overall crop health. These radars provide attractive alternatives to the airborne radars due to their low cost and installation flexibility. Moreover, UAV radars operating in the microwave range have the capability to penetrate through different environmental targets and perform accurate measurements [1] [2]. For an UAV radar to effectively measure soil moisture and monitor vegetation, three main challenges need to be addressed. First, the overall payload of the system needs to be as low as possible; this is crucial to extend the flight time of the UAV and reduce the power consumption. Secondly, the maximum flight altitude- called the ambiguous range- should be higher than the natural obstacles in the field. Typically, in heavily vegetated areas, trees can reach up to 40 m in height. So, to secure safe and easy access for the UAV, the radar should have the capability to operate at sufficient altitude. Finally, the radar range resolution depends on its operating bandwidth [3]. Thus, UWB radars with 20% bandwidth or more are desirable.

Recently, many research proposed different radar systems to fulfill the foregoing requirements. Tan et al. [4] and Jessen et al. [5], designed an UWB and lightweight UAV radar systems for snow depth measurements using a vector network analyzer (VNA) to generate the signal with total payload between 3-4 kg. Similarly, Wu et al. [6] presented another lightweight ground penetrating radar (GPR) based on a VNA for soil moisture mapping with 200 MHz bandwidth. Additionally, Noviello et al. [7] also installed an UWB pulse radar on a UAV. However, all of the above radars had a limited flight altitude that varied between 1 and 15 m. This limitation prevents such systems from operating in heavily vegetated areas. Lort et al. [8], alternatively, described a UAV radar operating at 100 m altitude, but their radar requires a transmit power of 30 dBm over a narrow band of 100 MHz. Recently, Simpson et al. [9] presented an UWB, FMCW radar that operates from 2 to 6 GHz and is integrated on a UAV to measure soil moisture at 100 m altitude. However, the overall weight of the radar is around 5 kg, which requires high power consumption.

In the last few years, the mm-wave frequencies have garnered more attention due to the ability of designing compact systems at this range. Many radar systems have been reported at these high frequencies [10]-[14]. However, the limited capability of penetrating through different objects limited their applications to automotive applications or range detection. On the other hand, the low cost of the mm-wave automotive sensors and the wide operating band of 76-81 GHz offer new solutions for radar development [15].

This letter provides a short description of a compact and lightweight FMCW radar for remote sensing applications using a commercially available mm-wave radar evaluation board. The mm-wave transmitted signal is down-converted into 3-5 GHz and the received signal is up-converted back to the mm-wave range to be processed by a data capture board. This approach enables us to obtain an UWB microwave radar with 850 g weight for the mm-wave sensor, data capture board, cables, and the RF part. The radar is operated up to 100 m altitude for more than 30 minutes to scan an area of 1.2×1.5 km^2.

II. CHIRP GENERATION AND FREQUENCY CONVERSION

Fig. 1 shows the simplified system block diagram. A mm-wave radar evaluation board from Texas Instruments (AWR1843) is used to generate the wideband chirp signal [16].

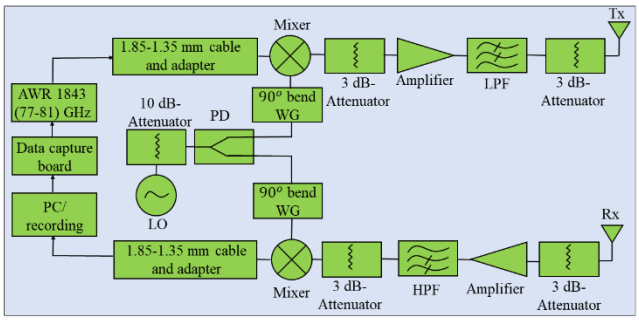

Fig. 1. Block diagram of the proposed radar system.

This work was supported in part by NOAA/UCAR under contract NA18NWS4620043B and NOAA/CISESS under contract NA19NES432000.

The authors are with the University of Alabama, Tuscaloosa, USA. [1] Electrical and Computer Engineering department [2] Aerospace Engineering and Mechanics department.

To process the collected data from the mm-wave sensor, a data capture board (DCA1000) is connected to the system. An E-band waveguide mixers and power divider with WR-12 ports are used to interface the mm-wave sensor. Also, a local oscilator is used to down-convert the mm-wave signal to the desired IF frequency range. After the signal is down converted, it is amplified, filtered, and supplied to the transmit antenna through a 3-dB attenuator. The attenuator is used to reduce the multiple reflections between the antenna and the next RF component in the chain. The interface between the mm-wave board and the designed system is performed by cutting the trace of the transmitter and receiver antenna arrays and inserting a 50 Ω coplanar waveguide (CPWG) on top of the evaluation board. The connection is then performed using wire bonding and attached on the side of the board to supply the signal to the mixer for down-conversion into the microwave range.

Fig. 2 shows the radar chirp characterization results. The integrated radar performance is evaluated using 100 m optical delay line as shown in Fig. 2(a). In the FMCW radar, the beat frequency signal obtained a sample of the transmit signal with received signal (which is accomplished in the mm-wave radar chip) that is directly proportional to the target range. The beat frequency signal from the radar chip is digitized and processed to target range and reflectivity characteristics. The time-domain signal containing beat frequencies proportional to range is weighted with a Hanning window before Fourier transformation. The resulting frequency data provide range and reflectivity information and the ideal Hanning window is compared with the radar signal. Fig. 2(b) shows the spectrogram of the time domain chirp over the bandwidth. The radar chirp has a low non-linearity of 0.005%, which represents the average of the deviation between the spectrogram line and a linear line from the start and end frequencies of the chirp [17].

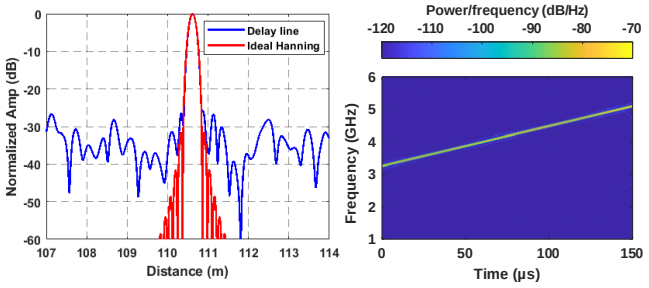

(a) (b)

Fig. 2. (a) Optical delay line impulse response (b) Spectrogram.

One of the advantages of using this mm-wave sensor to build the proposed radar is the fast-sweeping time. Basically, most of the automotive radars have a sweep time around 60-200 μs [15], [18]. This allows radar operation on both slow and fast moving platforms. In the proposed radar, the sweep time is set to 150 μs. In addition, due to their lightweight, low power consumption, interface simplicity and availability of data processing boards, these sensors are excellent candidates for a UAV radar applications.

III. Antenna Gain and Link Budget Analysis

For the link budget analysis, two possible scenarios were taken into consideration in our test: the nadir case and the 20° off-nadir case. Two identical (8×2) Vivaldi antenna arrays are used in the radar, where the gain (G) of each of them is varied from 15-18 dBi throughout the frequency of interest, as shown in Fig. 3. The distance between the antennas is set to be 1.3 m to achieve an isolation of -60 dB within the operating band.

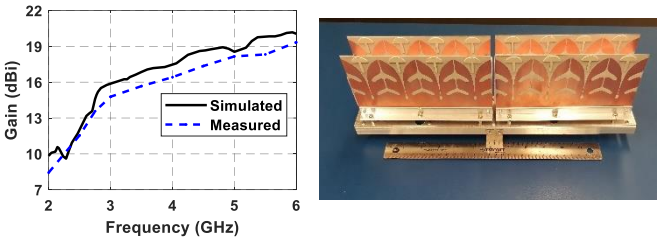

(a) (b)

Fig. 3. Antenna array (a) Peak realized gain (b) geometry and fabrication.

For the nadir case, the signal to noise ratio for a planar reflector is given by (1) [3] [19]:

$$SNR = \frac{P_t G^2 \lambda^2 |\Gamma|^2}{(4\pi)^2 (2R)^2 KTBN_F} \quad (1)$$

where, P_t is the transmitter output power, R is the radar range and Γ is the reflection coefficient; K is Boltzmann constant, T is the temperature in kelvin, B is the IF bin width, and N_F is the noise figure of the receiver. For a distributed target with unfocused Synthetic Aperture Radar (SAR) processing in the along-track direction and pulse limited case in the range direction, the signal to noise ratio is given by (2).

$$SNR = \frac{P_t G^2 \lambda^2 \sigma_o A}{(4\pi)^3 R^4 KTBN_F} \quad (2)$$

$$A = 0.5\sqrt{R\lambda}\frac{c}{2B\sin(\theta)} \quad (3)$$

where, A is the illuminated area in meters, σ_o is the radar cross section in meter, and θ is the incidence angle in radians or degrees. Based on the link budget analysis, the transmitted signal is amplified to 10 dBm. This power level is sufficient to obtain approximately 45 dB of *SNR* for the nadir case from the water surface at 100 m altitude. This represents the maximum possible received signal which should be taken into consideration when designing the radar to avoid receiver saturation. Also, the *SNR* for the off-nadir case from a dry ground surface is about 15 dB.

IV. Field Test Results

For the field measurements, the radar system is installed on the Dragon X6 multirotor UAV manufactured by XFold, as shown in Fig. 4. The power supply and RF system are positioned in a metal box and separated with a metal sheet to mitigate potential interference. Four different voltage outputs- 3.3, 5, 8 and 12 V- provide all necessary power to the electronic components. To prevent the receiver saturation with high received power from short ranges, a relay channel is added to turn on/off the radar amplifiers. The relay channel is connected to a trigger with +3.3 V installed on the UAV and will be activated remotely from the remote controlling unit after the UAV reaches to 40 m height from the ground level. The flights are performed autonomously using wave points navigator. The speed of the UAV is set to be 3 m/s. This speed gives sufficient stability in the flights and allows for more chirps to be averaged coherently as the

maximum number of coherently averaged chirps is inversely proportional to the speed [20].

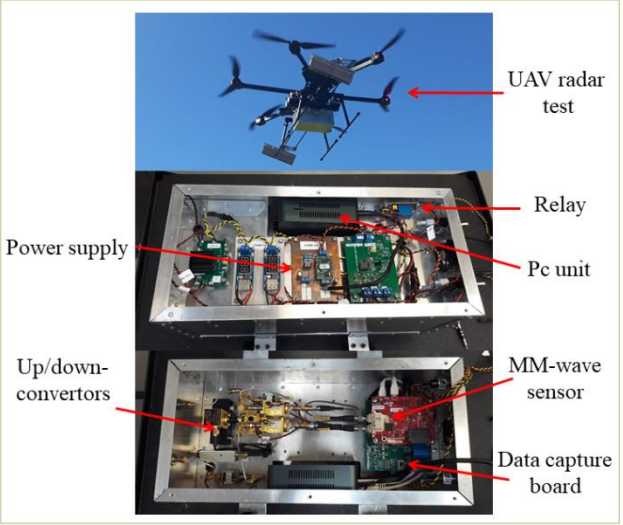

Fig. 4. Field test for the radar on the UAV with the radar box, power supply and RF components.

The radar data are processed with unfocussed Synthetic Aperture Radar (SAR) algorithm. To improve the SNR, 3000 chirps are coherently Integrated (CI) after applying Hanning widow. In addition, to reduce speckle, 7 along-track samples are incoherently averaged and then filtered with a 3×1 median filter to further improve image interpretability. Fig. 5 shows the echogram for the off-nadir antenna steering with 20°. The flight line included trees, surfaces covered by short grass, and a lake. During the flights, winds speed was low with a calm lake. This resulted in a very strong specular reflection and range sidelobes associated radar response that can be clearly seen over the lake. The aerial image of the flight path is shown in Fig. 6 to compare with the radar results.

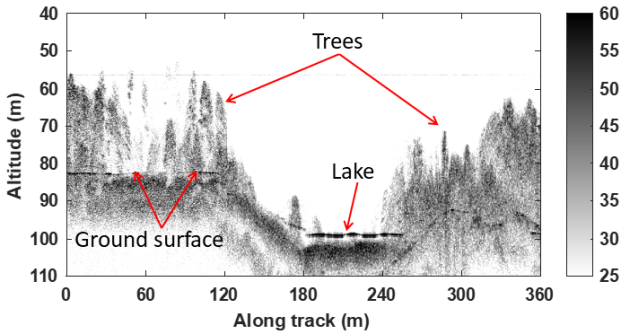

Fig. 5. Echogram in dB-scale from the proposed UAV radar system.

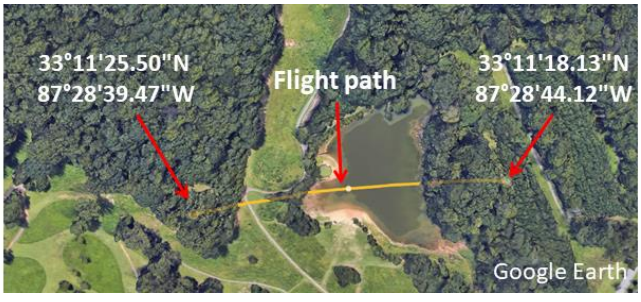

Fig. 6. Google earth aerial image for the flight line.

Fig. 7 shows the A-scope from the field test. The *SNR* is about 45 dB for the nadir case pointing to the water surface. After coherent integration, the *SNR* improved up to 67 dB. For the 20° off-nadir case, the received signal level is around -74 dBm with 22 dB *SNR*. After the coherent integration is applied to the raw data, the *SNR* is improved to 45 dB as shown in Fig. 5(b). Based on the link budget and the field test results, this radar can operate up to 300 m above the ground with a sufficient *SNR*.

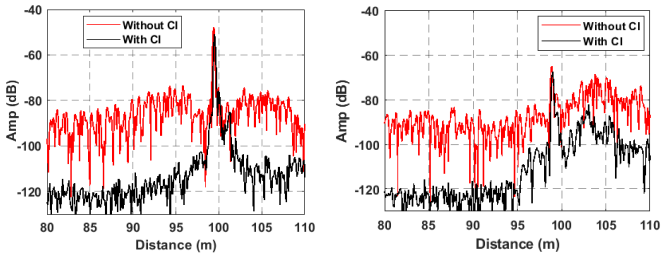

Fig. 7. A-scope from the water surface. (a) Nadir (b) 20° off-nadir.

The overall weight of the radar box is 2.5 kg which includes the mm-wave board, data capture board, up/down convertors, computer, power supply, power switches, fan units, mounting kits, and the radar box. This lightweight system enables one to fly the radar over a 1.2×1.5 km^2 area. The obtained wideband and high linearity of the radar chirps are crucial requirements to perform soil moisture and snow measurements. From the radar backscattering signals, the relative dielectric constant of the soil can be obtained [21] [22]. Table 1 illustrates the performance comparison between the proposed radar and the previous state of art. The total payload of the proposed radar is lighter than most of the previously reported systems that operate at the same altitude. Also, the transmitted signal power considered low for the operating range.

Table. 1. Comparison between the proposed radar and the previous radars.

Ref	BW (*MHz*)	T_x (*dBm*)	Altitude (*m*)	Tot. payload (*kg*)	Range resolution (*cm*)
[4]	5000	0	5-15	3	3
[5]	5000	-7	1	4	3
[6]	200	-3	1-5	1.5	750
[8]	100	30	100	6.5	1500
[9]	4000	16.7	100	5	5
[This work]	1900	10	100	2.5	7.9

V. CONCLUSIONS

A compact, lightweight FMCW radar for remote sensing is demonstrated. The radar uses a mm-wave automotive RF sensor and up/down-converts its center frequency from 80 GHz to 4 GHz while keeping a good linearity for the chirp. The radar is tested at a 100 m altitude on the UAV with a low output power. The radar raw data are processed with an unfocused SAR processor and shows the exact details of the flight path after comparison with the truth site details.

VI. ACKNOWLEDGEMENT

The authors would like to thank the Remote Sensing Center (RSC) students and faculty at the University of Alabama (UA) for their valuable help. Special thanks to Stephen Jones, Nathan Wagener, Aabhash Bhandari and Matthew Hargis.

REFERENCES

[1] A. Tan, K. Eccleston, I. Platt, I. Woodhead, W. Rack and J. McCulloch, "The design of a UAV mounted snow depth radar: Results of measurements on Antarctic sea ice," *2017 IEEE Conference on Antenna Measurements & Applications (CAMA)*, 2017, pp. 316-319, doi: 10.1109/CAMA.2017.8273437.

[2] K. S. Lyalin, A. A. Biryuk, A. Y. Sheremet, V. K. Tsvetkov and D. V. Prikhodko, "UAV synthetic aperture radar system for control of vegetation and soil moisture," *2018 IEEE Conference of Russian Young Researchers in Electrical and Electronic Engineering (EIConRus)*, 2018, pp. 1673-1675, doi: 10.1109/EIConRus.2018.8317425.

[3] Fawwaz Ulaby and David G. Long," *Microwave radar and radiometric Remote Sensing*," The University of Michigan Press, 2014.

[4] A. E. -C. Tan, J. McCulloch, W. Rack, I. Platt and I. Woodhead, "Radar Measurements of Snow Depth Over Sea Ice on an Unmanned Aerial Vehicle," *IEEE Transactions on Geoscience and Remote Sensing*, vol. 59, no. 3, pp. 1868-1875, 2021.

[5] R. O. R. Jenssen, M. Eckerstorfer and S. Jacobsen, "Drone-Mounted Ultrawideband Radar for Retrieval of Snowpack Properties," *IEEE Transactions on Instrumentation and Measurement*, vol. 69, no. 1, pp. 221-230, 2020.

[6] Kaijun Wu et al. "A new drone-borne GPR for soil moisture mapping," *Remote Sensing of Environment*, vol. 235, 2019.

[7] C. Noviello, G. Esposito, G. Fasano, A. Renga, F. Soldovieri, and I. Catapano, "Small-UAV Radar Imaging System Performance with GPS and CDGPS Based Motion Compensation," *Remote Sensing*, vol. 12, no. 20, p. 3463, 2020.

[8] M. Lort, A. Aguasca, C. López-Martínez and T. M. Marín, "Initial Evaluation of SAR Capabilities in UAV Multicopter Platforms," *IEEE Journal of Selected Topics in Applied Earth Observations and Remote Sensing*, vol. 11, no. 1, pp. 127-140, 2018.

[9] C. D. Simpson *et al*., "Development of A UAS-Based Ultra-Wideband Radar for Fine-Resolution Soil Moisture Measurements," *2021 IEEE Radar Conference (RadarConf21)*, pp. 1-4, 2021.

[10] B. Welp *et al*., "Versatile Dual-Receiver 94-GHz FMCW Radar System With High Output Power and 26-GHz Tuning Range for High Distance Applications," *IEEE Transactions on Microwave Theory and Techniques*, vol. 68, no. 3, pp. 1195-1211, 2020.

[11] S. -Y. Jeon *et al*., "W-Band MIMO FMCW Radar System With Simultaneous Transmission of Orthogonal Waveforms for High-Resolution Imaging," *IEEE Transactions on Microwave Theory and Techniques*, vol. 66, no. 11, pp. 5051-5064, 2018.

[12] V. Jain, F. Tzeng, L. Zhou and P. Heydari, "A Single-Chip Dual-Band 22–29-GHz/77–81-GHz BiCMOS Transceiver for Automotive Radars," *IEEE Journal of Solid-State Circuits*, vol. 44, no. 12, pp. 3469-3485, 2009.

[13] S. Kim *et al*., "Multichannel W-Band SAR System on a Multirotor UAV Platform With Real-Time Data Transmission Capabilities," *IEEE Access*, vol. 8, pp. 144413-144431, 2020.

[14] S. Gupta, P. K. Rai, A. Kumar, P. K. Yalavarthy and L. R. Cenkeramaddi, "Target Classification by mmWave FMCW Radars Using Machine Learning on Range-Angle Images," *IEEE Sensors Journal*, vol. 21, no. 18, pp. 19993-20001, 2021.

[15] C. Waldschmidt, J. Hasch and W. Menzel, "Automotive Radar — From First Efforts to Future Systems," *IEEE Journal of Microwaves*, vol. 1, no. 1, pp. 135-148, 2021.

[16] https://www.ti.com/product/AWR1843

[17] J. -B. Yan *et al*., "Airborne Measurements of Snow Thickness: Using ultrawide-band frequency-modulated-continuous-wave radars," *IEEE Geoscience and Remote Sensing Magazine*, vol. 5, no. 2, pp. 57-76, 2017.

[18] Z. Tong, R. Renter and M. Fujimoto, "Fast chirp FMCW radar in automotive applications," *IET International Radar Conference 2015*, pp. 1-4, 2015.

[19] R. K. Moore, "Ground echo," in Radar Handbook, M. I. Skolnik, Ed. New York: McGraw-Hill, 1970.

[20] K. Jin, T. Lai, Y. Wang, G. Li, and Y. Zhao, "Coherent Integration for Radar High-Speed Maneuvering Target Based on Frequency-Domain Second-Order Phase Difference," *Electronics*, vol. 8, no. 3, p. 287, 2019.

[21] Venkat Lakshmi, "Remote Sensing of Soil Moisture," *Hindawi Publishing Corporation*, vol. 2013, Article ID 424178, http://dx.doi.org/10.1155/2013/424178.

[22] C. N. Koyama, H. Liu, K. Takahashi, M. Shimada, M. Watanabe, T. Khuut, and M. Sato, "In-Situ Measurement of Soil Permittivity at Various Depths for the Calibration and Validation of Low-Frequency SAR Soil Moisture Models by Using GPR," *Remote Sensing*, vol. 9, no. 6, pp. 580, 2017.